# Systematic Assembly of a Full-Length Infectious Clone of Human Coronavirus NL63[∇]†

Eric F. Donaldson,[1,2]§ Boyd Yount,[2]§ Amy C. Sims,[2] Susan Burkett,[3]
Raymond J. Pickles,[1,3] and Ralph S. Baric[1,2]*

*Departments of Microbiology and Immunology[1] and Epidemiology[2] and Cystic Fibrosis/Pulmonary Research and Treatment Center,[3] University of North Carolina, Chapel Hill, North Carolina*

**Historically, coronaviruses were predominantly associated with mild upper respiratory disease in humans. More recently, three novel coronaviruses associated with severe human respiratory disease were found, including (i) the severe acute respiratory syndrome coronavirus, associated with a significant atypical pneumonia and 10% mortality; (ii) HKU-1, associated with chronic pulmonary disease; and (iii) NL63, associated with both upper and lower respiratory tract disease in children and adults worldwide. These discoveries establish coronaviruses as important human pathogens and underscore the need for continued research toward the development of platforms that will enable genetic manipulation of the viral genome, allowing for rapid and rational development and testing of candidate vaccines, vaccine vectors, and therapeutics. In this report, we describe a reverse genetics system for NL63, whereby five contiguous cDNAs that span the entire genome were used to generate a full-length cDNA. Recombinant NL63 viruses which contained the expected marker mutations replicated as efficiently as the wild-type NL63 virus. In addition, we engineered the heterologous green fluorescent protein gene in place of open reading frame 3 (ORF3) of the NL63 clone, simultaneously creating a unique marker for NL63 infection and demonstrating that the ORF3 protein product is nonessential for the replication of NL63 in cell culture. The availability of the NL63 and NL63gfp clones and recombinant viruses provides powerful tools that will help advance our understanding of this important human pathogen.**

Coronaviruses (CoVs) are the largest known single-stranded positive-sense RNA viruses; they encode 5′-capped, polyadenylated genomes ranging in size from 27 to 32 kb. Until recently, CoVs were predominantly associated with severe disease in domestic animals, including bovines (bovine CoV), swine (porcine epidemic diarrhea virus and transmissible gastroenteritis virus [TGEV]), avians (infectious bronchitis virus [IBV]) (2, 8, 30, 36), and mice (mouse hepatitis virus [MHV]) (42), while infections in humans were primarily associated with mild upper respiratory tract diseases caused by human CoVs (hCoVs) hCoV-229E and hCoV-OC43 (30). However, the identification of a novel CoV as the etiological agent responsible for severe acute respiratory syndrome (SARS), an atypical pneumonia with a 10% mortality rate (53), indicated that hCoVs are capable of causing severe disease in humans and that unidentified hCoVs continue to exist in nature. More-recent discoveries have led to the identification of two additional hCoVs: (i) HKU-1, which has been associated with chronic pulmonary disease in humans (32), and (ii) NL63, which has been associated with both upper and lower respiratory tract disease in children and adults worldwide (1, 5, 9–11, 13, 23, 27, 28, 57, 62, 63). In addition, NL63 has been associated with croup in infants and young children (45, 60, 61).

Croup is a disease caused by many different viruses which is characterized by the sudden onset of a distinctive barky cough, stridor, hoarse voice, and respiratory distress resulting from upper-airway obstruction (6). Croup accounts for roughly 250,000 hospitalizations each year in the United States, and cases severe enough to require hospitalization can be fatal (24). In addition, although understudied, hCoV infection can result in a particularly severe pneumonia in the elderly, as evidenced by an outbreak of hCoV-OC43 in a retirement community that was associated with an ~10% mortality rate (41).

Taxonomically, CoVs are classified as members of the order *Nidovirales*, family *Coronaviridae*, genus *Coronavirus* (14, 30, 37). Currently, the *Coronavirus* genus is further divided into three primary groups based upon serological and phylogenetic data. Among the hCoVs, group 1 contains NL63 and hCoV-229E, while group 2 strains include hCoV-OC43, HKU-1, and SARS-CoV (14). The CoVs are roughly 100 nm in diameter, are enveloped, and contain three core structural spikes, including a 180- to 190-kDa spike glycoprotein (S), a 26-kDa membrane glycoprotein (M), and an envelope protein (E) of ~9 kDa. The genomic RNA is surrounded by a helical nucleocapsid composed of the ~50- to 60-kDa nucleocapsid protein (N) (46).

Interestingly, despite large differences in S glycoprotein sequences (less than 50% identity at the nucleotide level) between SARS-CoV and NL63, both viral S glycoproteins have been reported to interact with human angiotensin-converting enzyme-2 (ACE2) as a receptor for docking and entry into cells (25, 34, 44, 52). Upon entry into the host cell, the genomic RNA is uncoated and immediately translated into two large

polyproteins (30, 36). The first two-thirds of the CoV genome encodes nonstructural replicase proteins in two overlapping open reading frames (ORFs). The final one-third of the genome consists of the structural proteins S, E, M, and N, as well as accessory proteins specific to different strains which are translated from a nested set of 3′ coterminal subgenomic mRNAs (30, 36). For NL63, there are six genes with a gene order of 5′-replicase-S-ORF3-E-M-N-3′, wherein gene 1 encodes the nonstructural replicase proteins, gene 2 encodes S, gene 3 encodes an accessory protein of unknown function known as ORF3, gene 4 encodes E, gene 5 encodes M, gene 6 encodes N, and an overlapping ORF6b has been predicted to encode an additional accessory protein of unknown function (47, 59). All CoV genomes contain group-specific genes in the final one-third of the genome, and many of these genes encode group-specific accessory proteins of undetermined function that are dispensable for replication (17, 68). Interestingly, ORF3 of NL63 encodes a 225-amino-acid protein that is homologous to ORF4 of hCoV-229E (53% similarity) and to ORF3A of SARS-CoV (23% similarity) (39), and both of these proteins have unknown functions.

Full-length cDNA constructs of CoV genomes have revolutionized reverse genetic applications in coronavirology (7, 66–68). The strategy employed by our laboratory has been to divide the genome into stable cDNA fragments flanked by native or engineered type IIS restriction endonuclease sites that form unique junctions at the ends of each fragment. In addition, a T7 promoter site is added to the first fragment (at the 5′ end of the genome) to enable in vitro transcription of the full-length cDNA fragment after ligation, and a poly(A) tail is included at the end of the last fragment (at the 3′ end). For assembly, the fragments are cleaved by restriction digestion, which removes the nonnative portion of the restriction site and sequence, leaving unique ends that allow for a seamless, unidirectional ligation of the full-length cDNA clone. Transcription of the full-length cDNA is driven by the T7 promoter, and the full-length infectious RNA is transfected into cells. The individual fragments can be easily stored and amplified, and the smaller cDNA sizes are more manageable for targeted mutagenesis studies. This infectious clone strategy has been successfully employed for TGEV (65), MHV strain A59 (67), hCoV SARS-CoV strain Urbani (66), and IBV (64).

In this study, we report and characterize the first full-length infectious clone of NL63 (icNL63). In addition, we replaced ORF3, which encodes a protein of unknown function, with the heterologous green fluorescent protein gene (GFP), simultaneously developing a new marker for NL63 infection and demonstrating that the protein product of ORF3 is nonessential for efficient viral replication in LLC-MK2 cells and primary cultures of human ciliated airway epithelium (HAE).

## MATERIALS AND METHODS

**Virus and cells.** The NL63 virus and LLC-MK2 cells were generously provided by Lia van der Hoek. The LLC-MK2 cell line is an epithelial line established in the 1950s from a pooled suspension prepared from kidney tissue of six adult rhesus monkeys (*Macaca mulatta*) (26). The LLC-MK2 cells were maintained at 37°C with 5% $CO_2$ in minimal essential medium supplemented with 10% fetal clone II (Gibco), 10% tryptose phosphate broth, and gentamicin (0.05 µg/ml)–kanamycin (0.25 µg/ml). NL63 was propagated on these cells, and the infections were maintained at 32°C in incubators maintained at 5% $CO_2$.

Human nasal and tracheobronchial epithelial cells were obtained from airway

TABLE 1. Primers used to generate infectious clone fragments and for PCR

| Primer | Nucleotide position | Comment |
|---|---|---|
| 5′T7NL63+ | 5′ end of genome | Creates 5′ T7 RNA polymerase promoter |
| NL63:A− | 6907–6928 | Creates BsmBI junction between A and B |
| NL63:B+ | 6922–6948 | Creates BsmBI junction between A and B |
| NL63:B− | 13537–13562 | Creates BsmBI junction between B and C |
| NL63:C+ | 13556–13579 | Creates BsmBI junction between B and C |
| NL63:C− | 19988–20011 | Creates BsmBI junction between C and D |
| NL63:D+ | 19991–20014 | Creates BsmBI junction between D and D |
| NL63:D− | 23845–23875 | Creates BstAPI junction between D and E |
| NL63:E+ | 23854–23882 | Creates BstAPI junction between D and E |
| NL63:E− | 3′ end of genome | Creates 3′ poly(A) tail at end of genome |
| NL63-N1s | Leader sequence | Real-time PCR primer |
| NL63-N1a | 69–47 antisense of N | Real-time PCR primer for 116-nt amplicon |
| NL63-NR | 255–236 antisense of N | RT-PCR primer (with NL63-N1s) for 302-nt amplicon |
| NL63-7+3002 | 23582–23599 genomic | ~350 nt 5′ of BstAPI site |
| NL63-7R | 24490–24471 antisense genomic | ~650 nt 3′ of BstAPI site |

specimens resected from patients undergoing elective surgery under UNC Institutional Review Board-approved protocols by the UNC Cystic Fibrosis Center Tissue Culture Core. Briefly, primary cells were expanded on plastic to generate passage 1 cells and plated at a density of 250,000 cells per well on permeable Transwell-Col (12-mm diameter) supports (18, 43). HAE cultures were generated by the provision of an air-liquid interface for 4 to 6 weeks to form well-differentiated, polarized cultures that resemble in vivo pseudostratified ciliated epithelium (43).

**Design of the icNL63 and icNL63gfp clones.** Initial attempts at generating a synthetic NL63 clone based upon the genomic NL63 sequence originally deposited in GenBank in June 2004 with accession number NC_005831 were unsuccessful. However, this sequence was later updated with several corrections (NC_005831.2); these corrections were engineered into the synthetic clone, but we were still unable to successfully rescue recombinant virus. We then acquired the virus (as a kind gift from Lia van der Hoek), sequenced it, and attempted to generate the clone from this sequence, but yet again were unsuccessful at rescuing recombinant virus. This viral sequence was different from NC_005831.2 at six positions, and this viral stock was later determined to be problematic. A second shipment of virus was requested and used to successfully generate the clone described here (FJ211861). It is important to note that the NL63 genome is AT rich (66%), which likely contributed to problems with cloning and sequencing.

Once a reliable virus sample and sequence were established, icNL63 was amplified from viral cDNA (FJ211861) and cloned as a set of five fragments (Table 1). The first fragment, NL63-A, was PCR amplified using primer set 5′T7NL63+ (5′-GGTACCTAATACGACTCACTATAGCTTAAAGAATTTTTCTATCTATAG-3′) and NL63:A− (5′-GCGGCCGCGTCTCCAGGAGCTGTGGGTTGAACAG-3′). These primers created a T7 RNA promoter at the 5′ end of the fragment and a BsmBI restriction site at the 3′ end, respectively. The PCR product was gel isolated and then cloned into the pCR-XL TOPO cloning vector (Invitrogen). The second fragment, NL63-B, was amplified using primers NL63:B+ (5′-GCGGCCGCGTCTCCTCCTGCATATGTTATTATTGATAAG-3′) and NL63:B− (5′-GCGGCCGCGTCTCTGCTGGGGAAGAAGCTATTATCAAG-3′). Fragment NL63-C was amplified with primers NL63:C+ (5′-GCGGCCGCGTCTCCCAGCACTCGTTGATCAACGCAC-3′) and NL63:C− (5′-GCGGCCGCGTCTCTCTTTAGAGACATTTTCACCATC-3′). Both of these fragments, which are flanked with
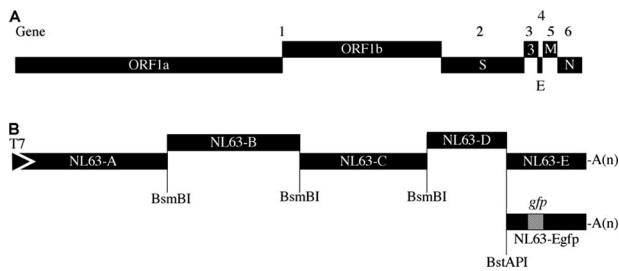
FIG. 1. The gene order of NL63 and the strategies used to generate the infectious clones. (A) The NL63 genome contains six genes, with ORF1a and -b encoding the viral nonstructural proteins involved primarily in replication. Genes 2 to 6 encode the structural and accessory proteins, with ORF3 (gene 3) encoding a protein of unknown function. (B) The NL63 genome was divided into five cDNA fragments (designated NL63-A to NL63-E) flanked by unique type IIS restriction endonuclease sites that enable a seamless, unidirectional assembly of the entire genome. Fragment NL63-A contains a T7 promoter sequence and NL63-E a poly(A) tail [A(n)]. In addition, ORF3 was deleted and a heterologous *gfp* gene inserted in its place in the NL63-E fragment to form fragment NL63-Egfp, which was used to engineer an NL63 clone with GFP as a marker of infection.

BsmBI sites, were gel isolated and cloned into the Big Easy v2.0 linear cloning vector (Lucigen). Fragment NL63-D was amplified using primer NL63:D+ (5′-GGTGAAAACGTCTCTAAAGATGG-3′) and primer NL63:D− (5′-CAGCAGCACAGTATGCAGAAAAAGCAAACC-3′). This primer set created a BsmBI site at the 5′ end and a BstAPI restriction site at the 3′ end. The last fragment, NL63-E, was PCR amplified using primers NL63:E+ (5′-TTTCTGCATACTGTGCTGCTGCCAACTG-3′) and NL63: E− (5′-TTTTTTTTTTTTTTTTTTTGTGTATCCATATCAAAAACAATATCATTAACAAGTACC-3′) and contained a BstAPI site at its 5′ end. The BstAPI site at the NL63-D and NL63-E junction was engineered by silent mutagenesis into the genomic sequence such that it would be retained after ligation of the two fragments, providing a unique marker for confirming that recombinant viruses were derived from the cloned cDNA. The last two fragments, NL63-D and NL63-E, were gel purified and subsequently cloned into the pCR-XL TOPO vector. The 5′ approximately 630 bp of the NL63-E fragment was PCR amplified using the primer set NL63:E+ and Ngfp2− (5′-CCATTATTGAACGTGGACCTTTTC-3′). The gene encoding GFP was amplified with primer Ngfp1+ (5′-GAAAAGGTCCACGTTCAATAATGGTGAGCAAGGGCGAGG-3′) and primer Ngfp3− (5′-GGTCACCTTACTTGTACAGCTCGTCCATG-3′). These two amplicons were joined in an overlapping extension PCR, and the resulting product was cloned into the pCR-XL cloning vector. A consensus clone was generated by using standard recombinant DNA techniques, and the BstAPI to BstEII fragment from this clone was inserted into the NL63-E fragment, which had also been digested with BstAPI and BstEII. The resulting plasmid then contained *gfp* in place of the NL63 ORF3, and this fragment was designated NL63-Egfp (Fig. 1).

**Systematic assembly of full-length NL63 cDNAs for icNL63 and icNL63gfp.** For assembling the infectious clones, plasmids incorporating cDNA fragments NL63-A through NL63-E were transformed into chemically competent Top 10 cells (Invitrogen) by heat shock at 42°C for 2 min and then plated on Luria Bertani (LB) plates with appropriate selection (kanamycin [25 μg/ml] or chloramphenicol [20 μg/ml]). Colonies were picked and grown under appropriate selection conditions in 5 ml of LB broth maintained at 28.5°C for 16 to 24 h and then purified and screened by restriction digestion. Larger 20-ml stocks were grown at 28.5°C for 24 h to 48 h for each of the cDNAs. Purified plasmids were then digested as follows: NL63-A, NL63-B, and NL63-C were digested with BsmBI, and NL63-D and NL63-E were digested under the appropriate conditions with BsmBI and BstAPI. NL63-Egfp was digested with BstAPI and BsmBI. Of note, the fragment boundaries were established by trial and error, as toxic regions in the genome prevented the cloning of several preliminary fragments.

After digestion, fragments were electroporated on 0.8% (wt/vol) agarose gel, and appropriate bands were excised and gel purified by using a Qiaex II gel extraction kit (Qiagen) with modifications (67). Briefly, all fragments were resuspended in 620 μl of QXI buffer, 11 μl Qiaex II silica gel particles, and 12.5 μl 3 M sodium acetate and eluted in 35 μl of elution buffer heated to 70°C. Purified fragments NL63-A through NL63-E were ligated by using T4 DNA ligase (Promega) overnight at 4°C in a total reaction mixture volume of ~200 μl to generate the wild-type (wt) icNL63. For the NL63 clone expressing GFP (icNL63gfp), the NL63-Egfp fragment was used instead of the NL63-E fragment.

**Transfection of full-length transcripts.** The full-length cDNAs were then further purified by chloroform extraction and isopropanol precipitation, transcribed using a T7 transcription kit (Ambion/Applied Biosystems), cotransfected into $8 \times 10^6$ LLC-MK2 cells in parallel with the N gene driven by an SP6 promoter, and transcribed with an SP6 transcription kit (Ambion/Applied Biosystems). LLC-MK2 cells were efficiently transfected with one pulse at 200 V and 950 μferrads using a Bio-Rad (Hercules, CA) Gene Pulser Xcell electroporator. Electroporated LLC-MK2s were plated in T25 flasks and incubated at 32°C for up to 7 days.

**Detection of recombinant NL63 and NL63gfp replication.** To determine if replication occurred in the icNL63-transfected cultures, cells were examined at regular intervals for cytopathic effect (CPE). However, CPE was not definitive at 7 days posttransfection, so half of the cells and supernatants were passaged with fresh cells and media, and cultures observed for an additional 7 days, prior to a third passage. At each passage, infected cells were harvested in Trizol reagent, total RNA was isolated, and reverse transcriptase PCR (RT-PCR) targeting subgenomic RNA was conducted using primers specific to the leader sequence and the 5′ end of the N gene (Table 1). Briefly, viral RNA was reverse transcribed to cDNA by using SuperScript III (Invitrogen) with modification to the protocol as follows. Random hexamers (300 ng) and total RNA (5 μg) were incubated for 10 min at 70°C. The remaining reagents were then added according to the manufacturer's recommendation, and the reaction mixture was incubated at 55°C for 1 h followed by 20 min at 70°C to deactivate the RT. For RT-PCR, a forward primer in the leader sequence (NL63-N1s, GATAGAGAATTTCTTATTTTAGACTTTGTG) and a reverse primer ~250 nucleotides (nt) into the N gene (NL63-NR, AGGTCCAGTACCTAGGTAAT) were used to generate a 302-bp product by PCR (Table 1).

Real-time RT-PCR was also conducted with the same cDNA templates by using a SmartCycler II (Cepheid) with Sybr green (diluted to 0.25×; Cepheid) to detect subgenomic cDNA with primers (7.5 pM) optimized to detect 116 nt spanning from the leader sequence (NL63-N1s; GATAGAGAATTTCTTAT TTAGACTTTGTG) to the 5′ end of the N gene (NL63-N1a; CATGTAAAAT GAAGGAGGAGGAA) (Table 1). The cDNA from the RT reaction of each virus was used at a volume of 2 μl for each reaction mixture, with a total reaction mixture volume of 25 μl. Omnimix beads (Cepheid) containing all reagents except Sybr green, primers, and template were used to standardize the reaction conditions. In addition, all products were verified by melting curve analysis.

For icNL63gfp, replication was confirmed by observing GFP fluorescence. Infections were passaged as described above until nearly 100% of cells were GFP positive, at which time the supernatants and cells were harvested. Replication was further verified by RT-PCR, using primers specific to subgenomic N transcripts.

**Plaque purification and titration of rescued virus.** Supernatants harvested from passage 3 of the transfections were diluted 1:10, and 200 μl of dilutions from $10^0$ to $10^{-5}$ were poured onto LLC-MK2 cells in six-well plates. After a 1-h adsorption period, 5 ml of overlay (0.8% [wt/vol] LE agar [Lonza, Inc.], 10% fetal clone II, 40% 2× minimal essential medium, 1% gentamicin-kanamycin) was added to each culture, and the infections were maintained at 32°C for 7 days. To help visualize the plaques, the plates were stained with neutral red for 1 h at 32°C, and five plaques were picked for each virus. Each plaque was incubated in phosphate-buffered saline (PBS) at 32°C for 30 min and then poured onto fresh LLC-MK2 cells and grown at 32°C for up to 9 days to allow for the propagation of purified virus. For the NL63gfp recombinant virus, plaques were clearly visible by fluorescent microscopy, and five plaques were picked and propagated as described above. The titers for both recombinant icNL63 and recombinant icNL63gfp were determined by plaque assay using LLC-MK2 cells. Briefly, LLC-MK2 cells were infected in duplicate with 200 μls of each serial dilution of $10^0$ to $10^{-5}$ of recombinant icNL63 or recombinant icNL63gfp in six-well plates with a 1-h adsorption period. Five milliliters of overlay (0.8% [wt/vol] LE agar [Lonza, Inc.], 10% fetal clone II, 40% 2× minimal essential medium, 1% gentamicin-kanamycin) was added to each infection, and the plates were maintained at 32°C until plaques were observed (between 4 and 7 days). To visualize plaques, plates were stained with neutral red for 2 h at 32°C and then incubated overnight prior to counting.

**Detection of marker mutations.** A unique BstAPI restriction endonuclease site was engineered into both the icNL63 and icNL63gfp clone to facilitate the unidirectional ligation of the NL63-D and NL63-E fragments. This engineering introduced a unique but silent BstAPI restriction endonuclease site from position 23916 to 23925 of both clones. This site was used to verify that the plaque-purified viruses harvested originated from the infectious clones. Primers flanking

the marker mutation (NL63-7+3002 [ATAAGATTCAGGATGTTG] and NL63-7R [GCAACAACCACAACAACCTG]) (Table 1) were used to amplify this region of the genome of wt NL63, recombinant icNL63, and recombinant icNL63gfp by RT-PCR. In all cases, an ~1,000-bp PCR product was detected by electroporation on a 0.8% agarose gel, and the band for each virus was excised and gel purified by using a Qiaex II gel extraction kit (Qiagen) with modifications (67) as described above. Analysis of the genotype was conducted by restriction digestion of the 1,000-bp DNA with the BstAPI restriction endonuclease. Briefly, 25 μl of DNA for each virus was incubated with 1 μl BstAPI, 3 μl NEB (New England Biolabs) buffer 3, and 1 μl double-distilled water at 60°C for 2 h and then electroporated on a 0.8% agarose gel. The remaining 5 μl of DNA was used to sequence the fragment for genotype verification.

**Growth kinetics and RNA analysis.** For the growth curve analysis, LLC-MK2 cells were inoculated at a multiplicity of infection (MOI) of 0.003 PFU/cell in 12-well plates with a 1-h adsorption period, followed by three washes with PBS. Two milliliters of medium was added to each culture, and the infections maintained at 32°C. The supernatants were harvested, at 300 μl per time point with 300 μl of medium added back, at 0, 8, 24, 48, 72, 96, 120, 144, 168, and 192 h postinoculation (p.i.). The titer for each virus at each time point was determined by plaque titration in LLC-MK2 cells maintained at 32°C, as described above. For Northern blot analysis, total RNA was harvested in Trizol reagent (Invitrogen), following the manufacturer's protocol, from cells infected at an MOI of 0.003 PFU/ml and harvested at 96 h p.i. The total RNA was diluted, and 5 μg was used for each virus, including wt NL63, recombinant icNL63, and recombinant icNL63gfp. The RNA from each infection was separated by gel electrophoresis, transferred to a nitrocellulose membrane, and probed with a 31-nt cDNA probe (3'-CTCTTGAACATTCCAATAACCAA*T*C*T*GC*T*CT-5'; N gene positions 151 to 180, italicized residues were biotinylated) designed to detect genomic and subgenomic RNAs by using a NorthernMax-Gly system (Ambion) following a modified protocol. Briefly, the exact procedure was followed up to and including the overnight 42°C hybridization of the probe to RNA cross-linked to the membrane. The next morning, the membrane was washed one time in low-stringency wash solution for 10 min, followed by a second wash in low-stringency wash solution at 45°C for 2 min. A third and final wash was conducted for 2 min at 45°C in a 50/50 mixture of high-stringency and low-stringency wash solutions. Detection of bands was accomplished by using a BrightStar BioDetect system (Ambion) following the manufacturer's protocol. The membrane was then exposed to film, which was prepared for publication by using Adobe Photoshop CS.

**IFA.** LLC-MK2 cells were grown to 70 to 80% confluence on four-well chamber slides (Lab-Tek, NUNC) and inoculated with recombinant icNL63 at an MOI of ~1 PFU/cell or mock inoculated (medium alone). At 48 h p.i., the medium was aspirated, and the cells were fixed and permeabilized in −20°C methanol overnight. The cells were rehydrated in PBS for 30 min and blocked in buffer comprised of PBS with 5% bovine serum albumin. All subsequent immunofluorescence assay (IFA) steps were conducted at 25°C in IFA assay wash buffer comprised of PBS containing 1% bovine serum albumin and 0.05% Nonidet P-40. After being blocked, the cells were incubated in the primary antibody, anti-N (anti-NL63 N; generously provided by Lia van der Hoek), diluted 1:1,000, for 1 h. The cells were then washed in IFA assay wash buffer three times at 10 min/wash. Next, the cells were incubated in the secondary antibody (goat anti-rabbit Alexa 488, diluted 1:1,000; Molecular Probes) for 45 min. Next, the cells were washed three times at 10 min/wash, followed by a final wash of 30 min in PBS. The cells were then visualized by fluorescent microscopy. The images were prepared for publication by using Adobe Photoshop CS.

**Western blotting.** LLC-MK2 cells were mock inoculated (medium alone) or inoculated with wt NL63, recombinant icNL63, or recombinant icNL63gfp at an MOI of 0.003, and at 144 h p.i., cells were washed in 1× PBS, lysed in buffer containing 20 mM Tris-HCl, pH 7.6, 150 mM NaCl, 0.5% deoxycholine, 1% Nonidet P-40, 0.1% sodium dodecyl sulfate (SDS) and postnuclear supernatants were added to an equal volume of 5 mM EDTA–0.9% SDS, resulting in a final SDS concentration of 0.5%. Equivalent sample volumes were loaded onto 4 to 20% Criterion gradient gels (Bio-Rad) and transferred to polyvinylidene difluoride membranes (Bio-Rad). The blots were probed with polyclonal rabbit antisera directed against the NL63 N protein (kindly provided by Lia van der Hoek) diluted 1:1,000 or with antisera directed against GFP (Clontech) diluted 1:1,000 and developed using chemiluminescence reagents (Amersham Biosciences).

**Inoculation of HAE cultures.** Prior to apical inoculation, the apical surfaces of HAE were rinsed three times over 30 min with PBS at 37°C, and inoculations were performed at 32°C with 200 μl of recombinant icNL63 or recombinant icNL63gfp virus stock (~10⁴ PFU/ml). Following a 2-h incubation at 32°C, the inoculant was removed, and HAE was maintained at 32°C for the remainder of the experiment. To generate growth curves at specific times after viral inoculation, 120 μl of tissue culture medium was applied to the apical surface of HAE

and collected after a 10-min incubation at 32°C. All samples were stored at −80°C until assayed for plaque formation on LLC-MK2 cells.

## RESULTS

**Design and assembly of icNL63 and icNL63gfp.** A full-length consensus sequence for NL63 was not possible, as all of the full-length sequences available at the National Center for Biotechnology Information (NCBI) differed significantly (see Fig. S1 in the supplemental material). Therefore, we sequenced the virus from an efficiently replicating stock and built the cDNA clone based upon this sequence (FJ211861). For icNL63, the NL63 genome was divided into five cDNA fragments (NL63-A through NL63-E) with unique type IIS endonuclease restriction sites flanking each junction (Fig. 1). For icNL63gfp, the same strategy was used, although the heterologous GFP gene was inserted in place of and under the control of the same transcriptional regulatory sequence as the accessory ORF3 in NL63-E, and this construct was designated NL63-Egfp (Fig. 1). To assemble the clones, the fragments were cut by restriction digestion (BsmBI and/or BstAPI) to remove the nonnative portion of the restriction site and sequence, leaving unique, asymmetrical sticky ends. The digested fragments were then ligated to generate the full-length cDNA clones, with NL63-Egfp being used instead of NL63-E for icNL63gfp (Fig. 1). A T7 promoter site engineered at the 5′ end of the genome in fragment NL63-A was used to drive in vitro transcription of the full-length cDNA to infectious RNA (Fig. 1). LLC-MK2 cells were transfected with the full-length RNA for each clone, and the cells monitored for CPE.

**Detection of recombinant icNL63 and recombinant icNL63gfp replication.** To determine if replication occurred in the icNL63 transfection cultures, cells were examined at regular intervals for CPE, which in LLC-MK2 cells is discernible as rounded cells that appear on top of the monolayer. In the case of recombinant icNL63, CPE was not conclusive at any time, but recovery of recombinant icNL63 was detected in passage 3 by RT-PCR amplification of leader-containing transcripts and further verified by an IFA with anti-N antibody and by plaque titration (Fig. 2A to D).

For recombinant icNL63gfp, replication was confirmed by observing GFP fluorescence following transfection or inoculation (Fig. 3). While fluorescent foci were observed as early as 2 days posttransfection at 32°C, additional passages at 7-day intervals were necessary to infect most of the cells in the culture. By 7 days p.i. of passage 3, there was obvious CPE in the recombinant icNL63gfp-infected cells (Fig. 3A). Cells and supernatants were harvested when nearly 100% of cells showed strong evidence of GFP fluorescence. Replication and the presence of viral subgenomic mRNA encoding viral structural proteins or GFP were further verified by RT-PCR (data not shown).

**Plaque purification and titration of rescued virus.** Viruses rescued from the icNL63 and icNL63gfp transfections were plaque purified, and stocks were propagated on LLC-MK2 cells. For recombinant icNL63, plaques were round and clear with an approximate diameter of 2.5 to 3 mm (Fig. 2). For recombinant icNL63gfp, plaques were clearly visible by fluorescent microscopy (Fig. 3D) and similar to recombinant icNL63, with the main difference observed between recombi-
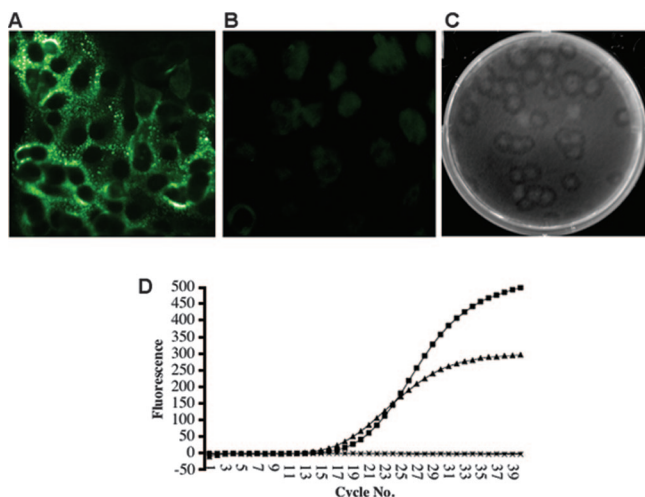
FIG. 2. Detection of replication in cells inoculated with icNL63 passage 3 supernatants. (A) Supernatants from the icNL63 transfection flask were used to inoculate four-well chamber slides of LLC-MK2 cells to assay for the presence of NL63 N protein by IFA. Nucleocapsid protein was detected in these cells, and it exhibited a perinuclear localization pattern. (B) In mock-infected cells, N protein is not detected. (C) While CPE was not dramatic, the supernatants from the icNL63 transfection resulted in various sizes of plaques. (D) Subgenomic transcription was verified by real-time RT-PCR by assaying for leader-containing transcripts. Amplification of the viral cDNA for wt NL63 (■) and recombinant icNL63 (▲) occurred at nearly identical cycle thresholds, suggesting that recombinant icNL63 generated quantities of subgenomic N gene that were similar to the quantities generated by wt NL63. LLC-MK2 cells (●) and the control without template (×) showed no amplification.
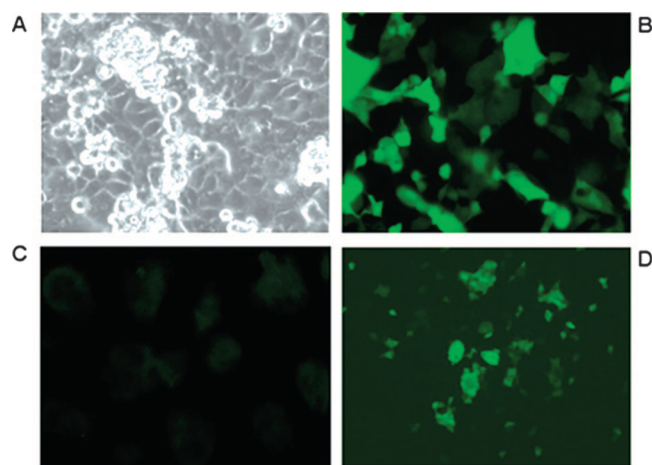


FIG. 3. Detection of replication in LLC-MK2 cells infected with icNL63gfp. (A) CPE was evident in cells transfected with icNL63gfp after passage 3, as indicated by rounded clumps of cells that grew on top of the monolayer, forming long continuous striations. (B) GFP fluorescence was detected as early as 24 h p.i.; however, the spread of GFP fluorescence to nearly every cell required three passages. (C) Cells infected with wt NL63 virus generated no detectable fluorescence beyond the normal background level. (D) Cells infected with recombinant icNL63gfp and covered with overlay medium formed plaques distinguished by fluorescent foci within the monolayer.

nant icNL63 and recombinant icNL63gfp plaques being one of definition, as the recombinant icNL63 plaques were clearly visible, while the recombinant icNL63gfp virus formed fuzzy plaques that were slightly smaller. Interestingly, all plaques for recombinant icNL63gfp were fluorescent. The viral titers derived from recombinant icNL63 plaques reached $2 \times 10^4$ PFU/ml in LLC-MK2 cells, while the titers for recombinant icNL63gfp were slightly higher, reaching a titer of $\sim 8 \times 10^4$ PFU/ml. The recombinant icNL63 virus titers were consistent with the peak virus titers reported previously for wt NL63 virus ($2 \times 10^5$ PFU/ml) (46, 47, 59).

**Detection of marker mutations in the rescued viruses.** As part of the cloning strategy, a silent BstAPI restriction endonuclease site was engineered into both the icNL63 and icNL63gfp clones at the NL63-D and NL63-E or NL63-Egfp junction to facilitate the unidirectional ligation of the NL63-D and NL63-E fragments. To verify that each clone had this marker mutation, viral RNA was harvested from cultures infected with plaque-purified stocks, and the $\sim 1,000$-nt region flanking the BstAPI site was amplified by RT-PCR (Fig. 4). In all cases, an $\sim 1,000$-nt PCR product was present following electroporation, and the band for each virus was excised and gel purified (Fig. 4). The purified 1,000-nt DNA from each virus was then digested with the BstAPI restriction endonuclease. Viral cDNA harvested from icNL63 and icNL63gfp recombinant viruses was digested into two bands of 600 nt and 400 nt, respectively (Fig. 4), while the wt NL63 viral cDNA was not cleaved by this enzyme (Fig. 4). Further, this region was

sequenced to verify that the marker mutation was present in the two clones, and this was the case for both recombinant viruses (Fig. 4).

**Growth kinetics and RNA analysis.** To determine if the recombinant viruses rescued from the two clones generated similar quantities of viral mRNAs, Northern blot analysis was performed (Fig. 5A). The results of this analysis demonstrated that while recombinant icNL63gfp did not generate amounts of viral mRNAs equivalent to those generated by wt NL63, it did contain a unique, appropriately sized mRNA indicative of GFP (Fig. 5A). To determine if the recombinant viruses generated from the two clones grew with growth kinetics similar to those of wt NL63, a growth curve analysis was conducted. In general, viral growth was similar for wt NL63 and both recombinant viruses, although recombinant icNL63 appeared to have a shorter lag phase than wt NL63 and recombinant icNL63gfp (Fig. 6).

**Analysis of recombinant viruses by Western blotting.** A Western blot analysis was conducted to compare the levels of viral protein expression of wt NL63, recombinant icNL63, and recombinant icNL63gfp by using antisera against NL63 N and GFP. While all three viruses generated detectable levels of N protein, there was an obvious reduction in the recombinant icNL63gfp lane, suggesting that this virus does not produce wt levels of viral proteins (Fig. 5C); only recombinant icNL63gfp expressed the 28-kDa GFP protein (Fig. 5B). These results are consistent with those of Northern blotting, which demonstrated that recombinant icNL63gfp is also deficient in RNA synthesis but generates a subgenomic RNA consistent with the GFP gene engineered into the clone (Fig. 5A). The recombinant icNL63 virus mimics wt NL63 in RNA synthesis and protein expression (Fig. 5A to C).
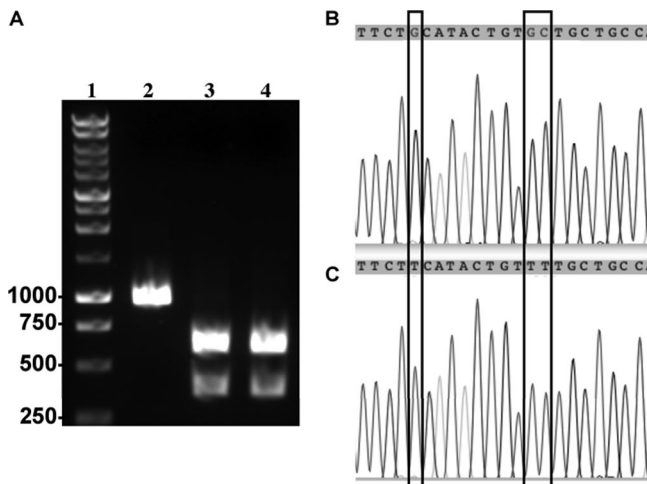
FIG. 4. Verification of the marker mutation in rescued virus from icNL63 and icNL63gfp. A silent BstAPI site introduced into both clones at the NL63-D and NL63-E or NL63-Egfp junctions was used to verify that the viruses rescued from the transfection flasks were generated from the cloned cDNA. (A) A 1,000-nt region flanking this site was amplified by PCR, digested by BstAPI, and analyzed by gel electrophoresis. Lane 1, marker; lane 2, wt NL63 was not cut by BstAPI; lane 3, the DNA from this region in the icNL63 recombinant virus was cleaved by BstAPI; and lane 4, the DNA from this region in the icNL63gfp recombinant virus was also cleaved by BstAPI. To verify the genotype, this region was sequenced for icNL63, icNL63gfp and wt NL63. Molecular sizes in nucleotides are shown on the left. (B) The chromatograms of icNL63 and icNL63gfp were identical in this region and are shown here. (C) The sequence chromatogram of wt NL63 in this region. The differences between the two chromatograms are indicated by the boxes. The BstAPI recognition site is GCANNNNNTGC.

**Recombinant NL63 infections in HAE cultures.** A primary target for infection by other hCoVs, like SARS-CoV and hCoV-229E, is ciliated cells (51) of the upper airways. As ciliated cells express robust levels of ACE2 (20), we next determined if the recombinant icNL63 and icNL63gfp viruses

could replicate efficiently in these cultures of HAE. The infection of HAE by recombinant icNL63gfp was detected as fluorescent cells on day 1 (24 h p.i.), and the fluorescence increased in intensity at each time point of the experiment (Fig. 7), although its spread to additional cells appeared to be limited (Fig. 7). In HAE, recombinant icNL63 CPE was not evident, although virus was isolated and determined to reach peak titers of $5 \times 10^4$ on day 4 (96 h p.i.). In contrast, recombinant icNL63gfp achieved peak titers of $7.5 \times 10^3$ on day 5 (120 h p.i.) (Fig. 7).

These results indicate that recombinant NL63 viruses derived from the cDNA clones replicated as efficiently as biologically derived NL63 and grew in LLC-MK2 cells and HAE and that the replacement of ORF3 with the *gfp* transgene allowed the expression of GFP in infected cells. While ORF3 appears to be nonessential in cell culture, there were differences in RNA synthesis, protein expression, plaque morphology, and growth in HAE that suggest that ORF3 may play an important undetermined role during in vivo infection.

## DISCUSSION

A reverse genetics system for NL63 provides a platform for studying this virus in depth and is a necessary component in the development of vaccine candidates, vaccine vectors, and therapeutics. In this study, we developed a reverse genetics system for NL63 and rescued recombinant NL63 viruses by utilizing the same cloning strategy employed to generated infectious clones of TGEV (65), MHV (67), IBV (7), and SARS-CoV (66). In general, plaque-purified wt NL63 and recombinant icNL63 viruses were indistinguishable in cell culture, as both generated nearly round plaques of 2.5 to 3 mm in diameter in LLC-MK2 cells (Fig. 2), exhibited similar levels of RNA synthesis and protein expression (Fig. 5), and replicated with similar growth kinetics (Fig. 6). Interestingly, although recombinant icNL63 appeared to have a shortened lag phase, this difference fell within the range of error for the experiment and
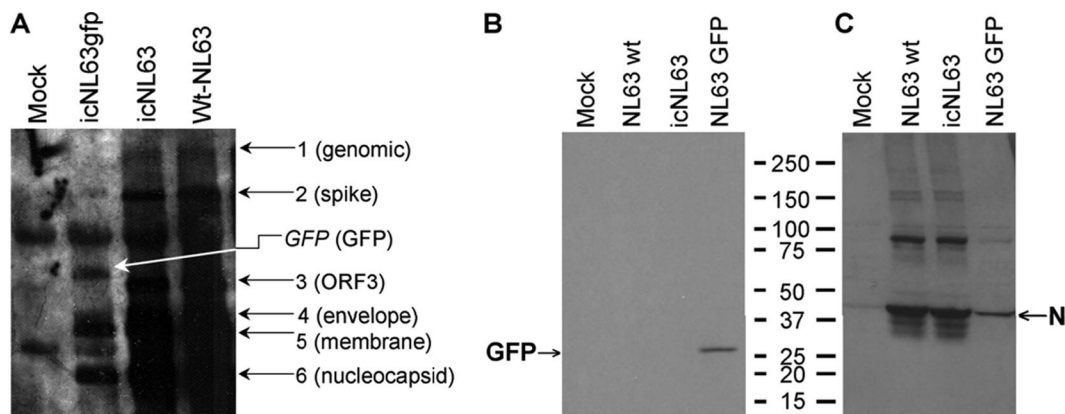


FIG. 5. Verification of replication by Northern and Western blotting. (A) A Northern blot analysis was conducted using viral RNA harvested from LLC-MK2 cells infected with wt NL63, recombinant icNL63, or recombinant icNL63gfp. Six bands were detected which correspond to the six viral genes. The protein product that arises from each gene is indicated in parentheses. The recombinant icNL63gfp virus produced an mRNA band that corresponds to the GFP transgene and lacked the mRNA corresponding to gene 3 (ORF3), whereas wt NL63 and recombinant icNL63 viruses produced the six expected viral RNAs. (B) A Western blot was conducted using the anti-GFP antibody to detect the GFP protein from infected-cell lysates, which was only detectable for the recombinant icNL63gfp virus. (C) A Western blot was conducted using the anti-N antibody to detect the N protein. N protein expression was reduced for the recombinant icNL63gfp virus. Molecular masses in kilodaltons are shown between the blots.
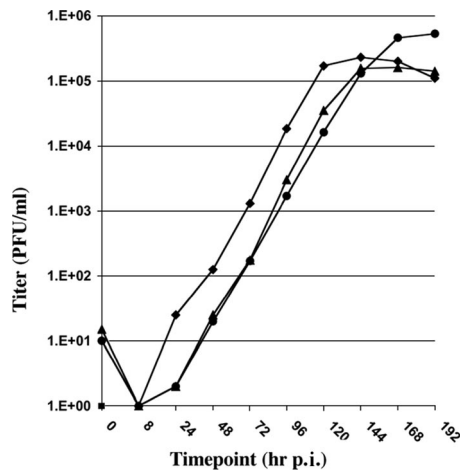
FIG. 6. Growth kinetics of wt NL63 and recombinant icNL63 and icNL63gfp viruses. All three viruses grew with similar growth kinetics, although recombinant icNL63 virus (◆) appeared to have a shorter lag phase. The growth kinetics of wt NL63 (●) and recombinant icNL63gfp (▲) were nearly identical at every time point until day 7 (168 h p.i.), when wt NL63 reached peak titers of $5 \times 10^5$ PFU/ml. Recombinant icNL63 reached a peak titer of $3 \times 10^5$ on day 6 (144 h p.i.), and recombinant icNL63gfp reached a titer of $1.5 \times 10^5$ PFU/ml on the same day. All virus titers at each time point fall within 1 standard deviation, suggesting that all titers are similar.
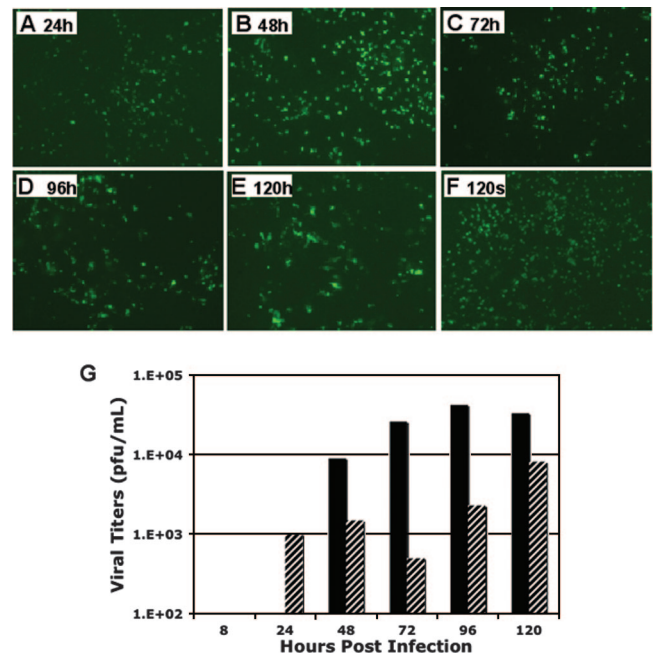


FIG. 7. Time course of infection of HAE and viral titers produced by recombinant icNL63 and icNL63gfp. HAE cultures were inoculated with recombinant icNL63 and recombinant icNL63gfp and monitored for 6 days. Fluorescence was detected in HAE infected with recombinant icNL63gfp by 24 h p.i. and continued to be detected throughout the course of the experiment. (A to E) Images showing the recombinant icNL63gfp-infected HAE at 24-h intervals beginning with the 24-h p.i. time point and continuing through 120 h p.i. (F) SARS-CoV-GFP-infected HAE cultures at 120 h p.i. produced smaller fluorescent foci. (G) Titers were determined for both recombinant icNL63 (black) and recombinant icNL63gfp (hatched) at each time point.

was likely due to differences in cell culture and not differences in the recombinant icNL63 virus (Fig. 6). In addition, recombinant icNL63 viral RNA contained the unique marker introduced into the clone sequence to allow verification that the virus was derived from the engineered clone (Fig. 4). To test the utility of this reverse genetics system, we removed the accessory ORF3 from the NL63 genome and replaced it with the gene for GFP, creating a unique system for monitoring NL63 infection in real time. In addition, the results of this experiment demonstrated that the ORF3 protein is nonessential for the replication of NL63 in LLC-MK2 cells. This observation was in agreement with the results of several other studies which have shown that CoV accessory and luxury ORFs are dispensable for in vitro replication (17, 66, 68).

The replacement of ORF3 with the heterologous GFP gene resulted in infected cells that were detectable by fluorescent microscopy (Fig. 3), and the recombinant icNL63gfp virus generated titers and exhibited growth kinetics that were essentially identical to those of wt NL63 and recombinant icNL63 in LLC-MK2 cells (Fig. 6). Interestingly, recombinant icNL63gfp virus generated plaques that were slightly smaller (2 to 2.5 mm in diameter versus 2.5 to 3 mm), with irregular borders, and were considerably less-well defined than wt NL63 plaques (data not shown). Although the different plaque phenotype did not correlate to a reduction in growth kinetics (Fig. 6), recombinant icNL63gfp had modestly reduced levels of RNA synthesis (Fig. 5A) and protein expression (Fig. 5C) compared to those of wt NL63. The lack of an animal model for studying NL63 made it impossible to determine if ORF3 plays a role in viral pathogenesis in vivo.

At the time of this study, 12 NL63 genomes containing a full-length ORF3 sequence were available at NCBI, and among these, ORF3 was strictly (100%) conserved at the

amino acid level in all isolates, while most ORF3 genes varied 1 to 2% at the nucleotide level. While this suggests an important role for the ORF3 protein product in vivo, ORF3 deletion from icNL63gfp was not deleterious to replication in LLC-MK2 cells. This finding was not surprising given that the distantly homologous proteins ORF4 in hCoV-229E (12) and ORF3a in SARS-CoV (17, 68) have also been shown to be nonessential in cell culture. Group-specific ORFs of several different CoVs have been deleted, and while some deletions attenuated pathogenesis or viral growth in vitro, the function of most is unknown. Two exceptions are the ORF3b and ORF6 products of SARS-CoV, which have been characterized as interferon antagonists (16, 29). Whether ORF3 of NL63 encodes interferon antagonist activities remains to be determined. In preliminary studies, we have observed that GFP-tagged ORF3 protein localizes to the nucleus when transfected into cells (data not shown).

In addition to the transfection of LLC-MK2 cells, recombinant icNL63 and recombinant icNL63gfp were used to infect primary HAE, which supports the infection and spread of other respiratory pathogens, such as influenza virus, respiratory syncytial virus (RSV), SARS-CoV, and paramyxoviruses (4, 49–51, 56, 69). Since NL63 infects both the upper and lower respiratory tracts and HAE cultures maintain the form and function of human ciliated airways, these cultures represent a relevant and authentic model for studying this virus. Not sur-

prisingly, both recombinant viruses grew in HAE (Fig. 7G), and recombinant icNL63gfp was detectable by fluorescence by 24 h p.i. with increased fluorescent intensity over time, although its spread from cell to cell was somewhat limited (Fig. 7A to E). In contrast, SARS-CoV expressing GFP in an accessory ORF was used to infect HAE cultures, and spreading of this virus was evident over the course of the infection (Fig. 7G). Spreading of RSV in HAE has also been observed (70). Interestingly, the fluorescent foci detected with recombinant icNL63gfp infection were smaller and generally more diffuse than those observed in HAE infected with the recombinant SARS-CoV expressing GFP (Fig. 7F) (50). Although this may be due to variability between cultures, we cannot rule out the possibility that ORF3 is nonessential for replication in LLC-MK2 cells but may play a role in more-relevant tissues that are related to replication in nonimmortalized cell lines. The results of previous studies have shown that parainfluenza virus and RSV infection of HAE mimic their in vivo replication capacities, while in cell lines, attenuation is not seen (69, 70). We speculate that ORF3 might be required for efficient viral egress in HAE, as spreading within cultures was reduced in the recombinant icNL63gfp virus. This is supported by the fact that recombinant icNL63gfp appeared to grow less efficiently than recombinant icNL63 in HAE (Fig. 7G).

Engineering GFP into icNL63 and rescuing recombinant viruses expressing this marker protein provides an important reagent enabling the testing of drugs and therapeutic agents against infections in real time. Several other viral systems have utilized a similar approach to generate novel reagents which allow high-throughput therapeutic screening (3, 15, 19, 22, 31, 33, 35, 38, 54, 58). In LLC-MK2 cells, we observed viral spread throughout the culture, even though there were no detectable differences in CPE. While only a few fluorescent foci were present at early times posttransfection, over time we observed more and more fluorescence spreading to neighboring cells. Fluorescence was also detectable in the HAE, providing a platform to monitor the infection of primary HAE in real time. Importantly, in all cases the GFP transgene was highly stable in the NL63 genome for over 2 months in culture, an important feature for the development of hCoV vaccine vectors.

All hCoVs, with the exception of SARS-CoV, grow poorly in cell culture, while some, including hCoV-OC43 and hCoV-229E, do not generate plaques, making downstream assays difficult to perform. Moreover, a new hCoV associated with pneumonia in adults, known as HKU-1, has never been successfully cultured in vitro. Poor growth in culture makes it extremely difficult to rescue recombinant viruses from full-length cDNA clones, which makes manipulating these virus genomes difficult. NL63 has an intermediate growth phenotype in cell culture, where it grows at an optimal temperature of 32°C, requiring 7 days to reach peak titer in LLC-MK2 cells, while SARS-CoV grows at 37°C with a distinct growth advantage, allowing it to reach peak titers in <48 h p.i. in Vero cells. These observations indicate that more-robust culture systems are needed for the development of NL63 as a vaccine vector for human use.

There are several distinct features that suggest that NL63 would be an efficacious vaccine vector, and these include (i) natural targeting of respiratory pathogen antigens to the appropriate mucosal epithelial cells lining the upper airways for optimal mucosal immune induction; (ii) virus induction of robust humoral, mucosal, and possibly cellular immune responses; and (iii) a genome size, organization, and helical nucleocapsid assembly scheme that allow (a) coordinated gene expression; (b) the deletion of luxury genes that are nonessential for replication; and (c) stable incorporation of multiple, large gene inserts (17, 66, 68). As a proof of principle, in this report we demonstrated that replacing the luxury ORF3 with heterologous gfp allowed stable targeting of GFP to the cells infected by NL63. Hypothetically, multiple heterologous antigens with novel transcriptional regulatory sequences could be engineered into the intergenic space between a propagation-deficient set of structural genes, providing a multivalent, replication-competent, propagation-deficient virus vector vaccine approach capable of immunizing against multiple viruses simultaneously. The complementation of such a vector in cells expressing the propagation-deficient gene could be utilized to assemble viable viruses that would act as one-hit vectors, generating antigen at the targeted cell while lacking the necessary components to generate a viable viral particle. A similar strategy was reported for TGEV whereby the E gene was expressed in a replicon cell system, which allowed the TGEV vaccine vector to be packaged as a viable virus and grown to high-titer replicon stocks (40). An NL63-based vaccine vector would potentially replicate extensively in the upper and, to a lesser extent, lower respiratory tract by targeting cell populations on mucosal surfaces that express ACE2, such as HAE, lung alveolar epithelial cells, and oral and nasal mucosa (21).

A current impediment in the field is the lack of either a small or large animal model of NL63 replication or pathogenesis. While mice express an ACE2 variant, virus replication has not been detected in mice infected with NL63. Moreover, the SARS-CoV receptor binding domain required adaptations in the spike protein to accommodate the structural differences imposed by the variations between the human and mouse ACE2 molecules (48). Since NL63 utilizes a different receptor binding domain and a different set of interactions, there may be even more changes necessary to adapt NL63 to replicate in mice. In addition, more-robust cell culture systems will be required for the propagation of NL63 as a vaccine vector system. In general, icNL63 makes a powerful vaccine platform, as CPE can be detected in LLC-MK2 cells; it may use the same receptor as has been described for SARS-CoV, a homologue of which is present in mice, and the stable expression of GFP will allow real-time monitoring of infections. These characteristics are in contrast to the hCoV-229E clone, which grows poorly and is difficult to detect by CPE (55).

The infectious clones described in this report provide a reverse genetics platform that can be used to develop candidate vaccine strains that might one day reduce the impact of NL63 as an important respiratory pathogen that infects children and adults worldwide. The benefits of such a vaccine would be to reduce the overall disease burden in children and perhaps reduce cases of croup. The availability of icNL63 and icNL63gfp provides research opportunities which will advance our understanding of in vivo tropisms and assist in the development of small and large animal models of infection. Moreover, detailed genetic manipulation of the genome will assist in understanding the role of viral genes in replication and patho-

genesis and lead to the development of hCoV-based vectored vaccines.

## REFERENCES

1. **Arden, K. E., M. D. Nissen, T. P. Sloots, and I. M. Mackay.** 2005. New human coronavirus, HCoV-NL63, associated with severe lower respiratory tract disease in Australia. J. Med. Virol. **75:**455–462.
2. **Baker, S. C.** 2004. Coronaviruses: from common colds to severe acute respiratory syndrome. Pediatr. Infect. Dis. J. **23:**1049–1050.
3. **Balliet, J. W., A. S. Kushnir, and P. A. Schaffer.** 2007. Construction and characterization of a herpes simplex virus type I recombinant expressing green fluorescent protein: acute phase replication and reactivation in mice. Virology **361:**372–383.
4. **Bartlett, E. J., M. Hennessey, M. H. Skiadopoulos, A. C. Schmidt, P. L. Collins, B. R. Murphy, and R. J. Pickles.** 2008. The role of interferon in the replication of human parainfluenza virus type 1 wild-type and mutant viruses in human ciliated airway epithelium. J. Virol. **82:**8059–8070.
5. **Bastien, N., K. Anderson, L. Hart, P. Van Caeseele, K. Brandt, D. Milley, T. Hatchette, E. C. Weiss, and Y. Li.** 2005. Human coronavirus NL63 infection in Canada. J. Infect. Dis. **191:**503–506.
6. **Bjornson, C. L., and D. W. Johnson.** 2008. Croup. Lancet **371:**329–339.
7. **Casais, R., V. Thiel, S. G. Siddell, D. Cavanagh, and P. Britton.** 2001. Reverse genetics system for the avian coronavirus infectious bronchitis virus. J. Virol. **75:**12359–12369.
8. **Cavanagh, D.** 2005. Coronaviruses in poultry and other birds. Avian Pathol. **34:**439–448.
9. **Chang, L. Y., B. L. Chiang, C. L. Kao, M. H. Wu, P. J. Chen, B. Berkhout, H. C. Yang, and L. M. Huang.** 2006. Lack of association between infection with a novel human coronavirus (HCoV), HCoV-NH, and Kawasaki disease in Taiwan. J. Infect. Dis. **193:**283–286.
10. **Choi, E. H., H. J. Lee, S. J. Kim, B. W. Eun, N. H. Kim, J. A. Lee, J. H. Lee, E. K. Song, S. H. Kim, J. Y. Park, and J. Y. Sung.** 2006. The association of newly identified respiratory viruses with lower respiratory tract infections in Korean children, 2000–2005. Clin. Infect. Dis. **43:**585–592.
11. **Dare, R. K., A. M. Fry, M. Chittaganpitch, P. Sawanpanyalert, S. J. Olsen, and D. D. Erdman.** 2007. Human coronavirus infections in rural Thailand: a comprehensive study using real-time reverse-transcription polymerase chain reaction assays. J. Infect. Dis. **196:**1321–1328.
12. **Dijkman, R., M. F. Jebbink, B. Wilbrink, K. Pyrc, H. L. Zaaijer, P. D. Minor, S. Franklin, B. Berkhout, V. Thiel, and L. van der Hoek.** 2006. Human coronavirus 229E encodes a single ORF4 protein between the spike and the envelope genes. Virol. J. **3:**106.
13. **Ebihara, T., R. Endo, X. Ma, N. Ishiguro, and H. Kikuta.** 2005. Detection of human coronavirus NL63 in young children with bronchiolitis. J. Med. Virol. **75:**463–465.
14. **Enjuanes, L., D. Cavanaugh, K. Holmes, M. Lai, H. Laude, P. Masters, P. Rottier, S. Siddell, W. Spaan, F. Taguchi, and P. Talbot.** 2000. *Coronaviridae*, p. 835–859. *In* Virus taxonomy. Classification and nomenclature of viruses. Academic Press, San Diego, CA.
15. **Fang, Y., R. R. Rowland, M. Roof, J. K. Lunney, J. Christopher-Hennings, and E. A. Nelson.** 2006. A full-length cDNA infectious clone of North American type 1 porcine reproductive and respiratory syndrome virus: expression of green fluorescent protein in the Nsp2 region. J. Virol. **80:**11447–11455.
16. **Frieman, M., B. Yount, M. Heise, S. A. Kopecky-Bromberg, P. Palese, and R. S. Baric.** 2007. Severe acute respiratory syndrome coronavirus ORF6 antagonizes STAT1 function by sequestering nuclear import factors on the rough endoplasmic reticulum/Golgi membrane. J. Virol. **81:**9812–9824.
17. **Frieman, M. B., B. Yount, A. C. Sims, D. J. Deming, T. E. Morrison, J. Sparks, M. Denison, M. Heise, and R. S. Baric.** 2006. SARS coronavirus accessory ORFs encode luxury functions. Adv. Exp. Med. Biol. **581:**149–152.
18. **Fulcher, M. L., S. Gabriel, K. A. Burns, J. R. Yankaskas, and S. H. Randell.** 2005. Well-differentiated human airway epithelial cell cultures. Methods Mol. Med. **107:**183–206.
19. **Ge, J. Y., Z. Y. Wen, Y. Wang, E. D. Bao, and Z. G. Bu.** 2006. Rescue of a recombinant Newcastle disease virus expressing the green fluorescent protein. Wei Sheng Wu Xue Bao **46:**547–551. (In Chinese.)
20. **Hamming, I., M. E. Cooper, B. L. Haagmans, N. M. Hooper, R. Korstanje,**

21. **A. D. Osterhaus, W. Timens, A. J. Turner, G. Navis, and H. van Goor.** 2007. The emerging role of ACE2 in physiology and disease. J. Pathol. **212:**1–11.
22. **Hamming, I., W. Timens, M. L. Bulthuis, A. T. Lely, G. J. Navis, and H. van Goor.** 2004. Tissue distribution of ACE2 protein, the functional receptor for SARS coronavirus. A first step in understanding SARS pathogenesis. J. Pathol. **203:**631–637.
22. **Hammoumi, S., C. Cruciere, M. Guy, A. Boutrouille, S. Messiaen, S. Lecollinet, and L. Bakkali-Kassimi.** 2006. Characterization of a recombinant encephalomyocarditis virus expressing the enhanced green fluorescent protein. Arch. Virol. **151:**1783–1796.
23. **Han, T. H., J. Y. Chung, S. W. Kim, and E. S. Hwang.** 2007. Human coronavirus-NL63 infections in Korean children, 2004–2006. J. Clin. Virol. **38:**27–31.
24. **Henrickson, K. J., S. M. Kuhn, and L. L. Savatski.** 1994. Epidemiology and cost of infection with human parainfluenza virus types 1 and 2 in young children. Clin. Infect. Dis. **18:**770–779.
25. **Hofmann, H., K. Pyrc, L. van der Hoek, M. Geier, B. Berkhout, and S. Pohlmann.** 2005. Human coronavirus NL63 employs the severe acute respiratory syndrome coronavirus receptor for cellular entry. Proc. Natl. Acad. Sci. USA **102:**7988–7993.
26. **Hull, R. N., W. R. Cherry, and O. J. Tritch.** 1962. Growth characteristics of monkey kidney cell strains LLC-MK1, LLC-MK2, and LLC-MK2 (NCTC-3196) and their utility in virus research. J. Exp. Med. **115:**903–918.
27. **Kaplan, N. M., W. Dove, S. A. Abd-Eldayem, A. F. Abu-Zeid, H. E. Shamoon, and C. A. Hart.** 2008. Molecular epidemiology and disease severity of respiratory syncytial virus in relation to other potential pathogens in children hospitalized with acute respiratory infection in Jordan. J. Med. Virol. **80:**168–174.
28. **Koetz, A., P. Nilsson, M. Linden, L. van der Hoek, and T. Ripa.** 2006. Detection of human coronavirus NL63, human metapneumovirus and respiratory syncytial virus in children with respiratory tract infections in southwest Sweden. Clin. Microbiol. Infect. **12:**1089–1096.
29. **Kopecky-Bromberg, S. A., L. Martinez-Sobrido, M. Frieman, R. A. Baric, and P. Palese.** 2007. Severe acute respiratory syndrome coronavirus open reading frame (ORF) 3b, ORF 6, and nucleocapsid proteins function as interferon antagonists. J. Virol. **81:**548–557.
30. **Lai, M. M., and D. Cavanagh.** 1997. The molecular biology of coronaviruses. Adv. Virus Res. **48:**1–100.
31. **Lambert, C., N. Thome, C. J. Kluck, and R. Prange.** 2004. Functional incorporation of green fluorescent protein into hepatitis B virus envelope particles. Virology **330:**158–167.
32. **Lau, S. K., P. C. Woo, C. C. Yip, H. Tse, H. W. Tsoi, V. C. Cheng, P. Lee, B. S. Tang, C. H. Cheung, R. A. Lee, L. Y. So, Y. L. Lau, K. H. Chan, and K. Y. Yuen.** 2006. Coronavirus HKU1 and other coronavirus infections in Hong Kong. J. Clin. Microbiol. **44:**2063–2071.
33. **Lee, K. W., and W. S. Tan.** 2008. Recombinant hepatitis B virus core particles: association, dissociation and encapsidation of green fluorescent protein. J. Virol. Methods. **151:**172–180.
34. **Li, W., J. Sui, I. C. Huang, J. H. Kuhn, S. R. Radoshitzky, W. A. Marasco, H. Choe, and M. Farzan.** 2007. The S proteins of human coronavirus NL63 and severe acute respiratory syndrome coronavirus bind overlapping regions of ACE2. Virology **367:**367–374.
35. **Liu, Y. L., S. L. Hu, Y. M. Zhang, S. J. Sun, A. Romer-Oberdorfer, J. Veits, Y. T. Wu, H. Q. Wan, and X. F. Liu.** 2007. Generation of a velogenic Newcastle disease virus from cDNA and expression of the green fluorescent protein. Arch. Virol. **152:**1241–1249.
36. **Masters, P. S.** 2006. The molecular biology of coronaviruses. Adv. Virus Res. **66:**193–292.
37. **McIntosh, K.** 1974. Coronaviruses: a comparative review. Curr. Top. Microbiol. Immunol. **63:**85–129.
38. **Moradpour, D., M. J. Evans, R. Gosert, Z. Yuan, H. E. Blum, S. P. Goff, B. D. Lindenbach, and C. M. Rice.** 2004. Insertion of green fluorescent protein into nonstructural protein 5A allows direct visualization of functional hepatitis C virus replication complexes. J. Virol. **78:**7400–7409.
39. **Muller, M. A.** 2007. Studies on human pathogenic coronaviruses: survey for coronaviruses in African bat species and characterization of the novel human coronavirus NL63 (HCoV-NL63) open reading frame 3 (ORF3). Freie Universität Berlin, Berlin, Germany.
40. **Ortego, J., D. Escors, H. Laude, and L. Enjuanes.** 2002. Generation of a replication-competent, propagation-deficient virus vector based on the transmissible gastroenteritis coronavirus genome. J. Virol. **76:**11518–11529.
41. **Patrick, D. M., M. Petric, D. M. Skowronski, R. Guasparini, T. F. Booth, M. Krajden, P. McGeer, N. Bastien, L. Gustafson, J. Dubord, D. Macdonald, S. T. David, L. F. Srour, R. Parker, A. Andonov, J. Isaac-Renton, N. Loewen, G. McNabb, A. McNabb, S. H. Goh, S. Henwick, C. Astell, J. P. Guo, M. Drebot, R. Tellier, F. Plummer, and R. C. Brunham.** 2006. An outbreak of human coronavirus OC43 infection and serological cross-reactivity with SARS coronavirus. Can. J. Infect. Dis. Med. Microbiol. **17:**330–336.
42. **Perlman, S.** 1998. Pathogenesis of coronavirus-induced infections. Review of pathological and immunological aspects. Adv. Exp. Med. Biol. **440:**503–513.
43. **Pickles, R. J., D. McCarty, H. Matsui, P. J. Hart, S. H. Randell, and R. C. Boucher.** 1998. Limited entry of adenovirus vectors into well-differentiated

airway epithelium is responsible for inefficient gene transfer. J. Virol. **72:** 6014–6023.

44. **Pohlmann, S., T. Gramberg, A. Wegele, K. Pyrc, L. van der Hoek, B. Berkhout, and H. Hofmann.** 2006. Interaction between the spike protein of human coronavirus NL63 and its cellular receptor ACE2. Adv. Exp. Med. Biol. **581:**281–284.

45. **Public Library of Science.** 2005. A novel virus for croup. PLoS Med. **2:**e274–e275.

46. **Pyrc, K., B. Burkhout, and L. van der Hoek.** 2005. Molecular characterization of human coronavirus NL63. Recent Res. Dev. Infect. Immun. **3:**25–48.

47. **Pyrc, K., M. F. Jebbink, B. Berkhout, and L. van der Hoek.** 2004. Genome structure and transcriptional regulation of human coronavirus NL63. Virol. J. **1:**7.

48. **Roberts, A., D. Deming, C. D. Paddock, A. Cheng, B. Yount, L. Vogel, B. D. Herman, T. Sheahan, M. Heise, G. L. Genrich, S. R. Zaki, R. Baric, and K. Subbarao.** 2007. A mouse-adapted SARS-coronavirus causes disease and mortality in BALB/c mice. PLoS Pathog. **3:**e5.

49. **Sheahan, T., B. Rockx, E. Donaldson, A. Sims, R. Pickles, D. Corti, and R. Baric.** 2008. Mechanisms of zoonotic severe acute respiratory syndrome coronavirus host range expansion in human airway epithelium. J. Virol. **82:**2274–2285.

50. **Sims, A. C., R. S. Baric, B. Yount, S. E. Burkett, P. L. Collins, and R. J. Pickles.** 2005. Severe acute respiratory syndrome coronavirus infection of human ciliated airway epithelia: role of ciliated cells in viral spread in the conducting airways of the lungs. J. Virol. **79:**15511–15524.

51. **Sims, A. C., S. E. Burkett, B. Yount, and R. J. Pickles.** 2008. SARS-CoV replication and pathogenesis in an in vitro model of the human conducting airway epithelium. Virus Res. **133:**33–44.

52. **Smith, M. K., S. Tusell, E. A. Travanty, B. Berkhout, L. van der Hoek, and K. V. Holmes.** 2006. Human angiotensin-converting enzyme 2 (ACE2) is a receptor for human respiratory coronavirus NL63. Adv. Exp. Med. Biol. **581:**285–288.

53. **Stadler, K., V. Masignani, M. Eickmann, S. Becker, S. Abrignani, H. D. Klenk, and R. Rappuoli.** 2003. SARS: beginning to understand a new virus. Nat. Rev. Microbiol. **1:**209–218.

54. **Tanaka, M., H. Kodaira, Y. Nishiyama, T. Sata, and Y. Kawaguchi.** 2004. Construction of recombinant herpes simplex virus type I expressing green fluorescent protein without loss of any viral genes. Microbes Infect. **6:**485–493.

55. **Thiel, V., J. Herold, B. Schelle, and S. G. Siddell.** 2001. Infectious RNA transcribed in vitro from a cDNA copy of the human coronavirus genome cloned in vaccinia virus. J. Gen. Virol. **82:**1273–1281.

56. **Thompson, C. I., W. S. Barclay, M. C. Zambon, and R. J. Pickles.** 2006. Infection of human airway epithelium by human and avian strains of influenza A virus. J. Virol. **80:**8060–8068.

57. **Vabret, A., J. Dina, S. Gouarin, J. Petitjean, V. Tripey, J. Brouard, and F. Freymuth.** 2007. Human (non-severe acute respiratory syndrome) coronavirus infections in hospitalised children in France. J. Paediatr. Child Health. **44:**176–181.

58. **van den Born, E., C. C. Posthuma, K. Knoops, and E. J. Snijder.** 2007. An infectious recombinant equine arteritis virus expressing green fluorescent protein from its replicase gene. J. Gen. Virol. **88:**1196–1205.

59. **van der Hoek, L., K. Pyrc, M. F. Jebbink, W. Vermeulen-Oost, R. J. Berkhout, K. C. Wolthers, P. M. Wertheim-van Dillen, J. Kaandorp, J. Spaargaren, and B. Berkhout.** 2004. Identification of a new human coronavirus. Nat. Med. **10:**368–373.

60. **van der Hoek, L., K. Sure, G. Ihorst, A. Stang, K. Pyrc, M. F. Jebbink, G. Petersen, J. Forster, B. Berkhout, and K. Uberla.** 2005. Croup is associated with the novel coronavirus NL63. PLoS Med. **2:**e240.

61. **van der Hoek, L., K. Sure, G. Ihorst, A. Stang, K. Pyrc, M. F. Jebbink, G. Petersen, J. Forster, B. Berkhout, and K. Uberla.** 2006. Human coronavirus NL63 infection is associated with croup. Adv. Exp. Med. Biol. **581:**485–491.

62. **Wu, P. S., L. Y. Chang, B. Berkhout, L. van der Hoek, C. Y. Lu, C. L. Kao, P. I. Lee, P. L. Shao, C. Y. Lee, F. Y. Huang, and L. M. Huang.** 2008. Clinical manifestations of human coronavirus NL63 infection in children in Taiwan. Eur. J. Pediatr. **167:**75–80.

63. **Xing, J. F., R. N. Zhu, Y. Qian, L. Q. Zhao, J. Deng, F. Wang, and Y. Sun.** 2007. Sequence analysis for genes encoding nucleoprotein and envelope protein of a new human coronavirus NL63 identified from a pediatric patient in Beijing by bioinformatics. Bing Du Xue Bao **23:**245–251. (In Chinese.)

64. **Youn, S., J. L. Leibowitz, and E. W. Collisson.** 2005. In vitro assembled, recombinant infectious bronchitis viruses demonstrate that the 5a open reading frame is not essential for replication. Virology **332:**206–215.

65. **Yount, B., K. M. Curtis, and R. S. Baric.** 2000. Strategy for systematic assembly of large RNA and DNA genomes: transmissible gastroenteritis virus model. J. Virol. **74:**10600–10611.

66. **Yount, B., K. M. Curtis, E. A. Fritz, L. E. Hensley, P. B. Jahrling, E. Prentice, M. R. Denison, T. W. Geisbert, and R. S. Baric.** 2003. Reverse genetics with a full-length infectious cDNA of severe acute respiratory syndrome coronavirus. Proc. Natl. Acad. Sci. USA **100:**12995–13000.

67. **Yount, B., M. R. Denison, S. R. Weiss, and R. S. Baric.** 2002. Systematic assembly of a full-length infectious cDNA of mouse hepatitis virus strain A59. J. Virol. **76:**11065–11078.

68. **Yount, B., R. S. Roberts, A. C. Sims, D. Deming, M. B. Frieman, J. Sparks, M. R. Denison, N. Davis, and R. S. Baric.** 2005. Severe acute respiratory syndrome coronavirus group-specific open reading frames encode nonessential functions for replication in cell cultures and mice. J. Virol. **79:**14909–14922.

69. **Zhang, L., A. Bukreyev, C. I. Thompson, B. Watson, M. E. Peeples, P. L. Collins, and R. J. Pickles.** 2005. Infection of ciliated cells by human parainfluenza virus type 3 in an in vitro model of human airway epithelium. J. Virol. **79:**1113–1124.

70. **Zhang, L., M. E. Peeples, R. C. Boucher, P. L. Collins, and R. J. Pickles.** 2002. Respiratory syncytial virus infection of human airway epithelial cells is polarized, specific to ciliated cells, and without obvious cytopathology. J. Virol. **76:**5654–5666.